5

Interferometric Processing

5.1 Interferogram Formation

Creating an interferogram from two single look complex (SLC) images involves two basic steps. The first step is to align the reference and repeat images to sub-pixel accuracy. This is done by two-dimensional cross-correlation (*xcorr* in GMTSAR) of hundreds of small sub-patches (e.g., 64×64) taken from the master and secondary images. A more modern approach is to use a topography grid and precise orbital information for alignment. Both approaches are described in Chapter 3. Then a six-parameter affine (or continuous) transformation is determined using a robust 2-D fit to the offset data (*fitoffset* in GMTSAR) or the precise orbit data as described in Chapter 3. This is used to align the secondary image to the master image. For raw data, the alignment is done in the SAR processor (*esarp* in GMTSAR). For SLC image data, the alignment is done using a sinc-interpolator (*resamp* in GMTSAR).

The second step is to multiply the two SLC images to form the complex interferogram. The complex number $C(\mathbf{x})$ in each pixel of the SLC image can be written as an amplitude $A(\mathbf{x})$ and phase $\phi(\mathbf{x})$ as

$$C(\mathbf{x}) = A(\mathbf{x})\, e^{i\phi(\mathbf{x})} \tag{5.1}$$

where $\mathbf{x} = (\rho, a)$ is the position vector consisting of range ρ and azimuth a. An interferogram is defined as

$$C_2 C_1^* = A_1 A_2 e^{i(\phi_2 - \phi_1)} = R(\mathbf{x}) + iI(\mathbf{x}) \tag{5.2}$$

The phase of the interferogram is extracted as

$$(\phi_2 - \phi_1) = \tan^{-1}\left(\frac{I}{R}\right) \tag{5.3}$$

An example of the phase of reference and repeat images and their phase difference is shown in Figure 5.1.

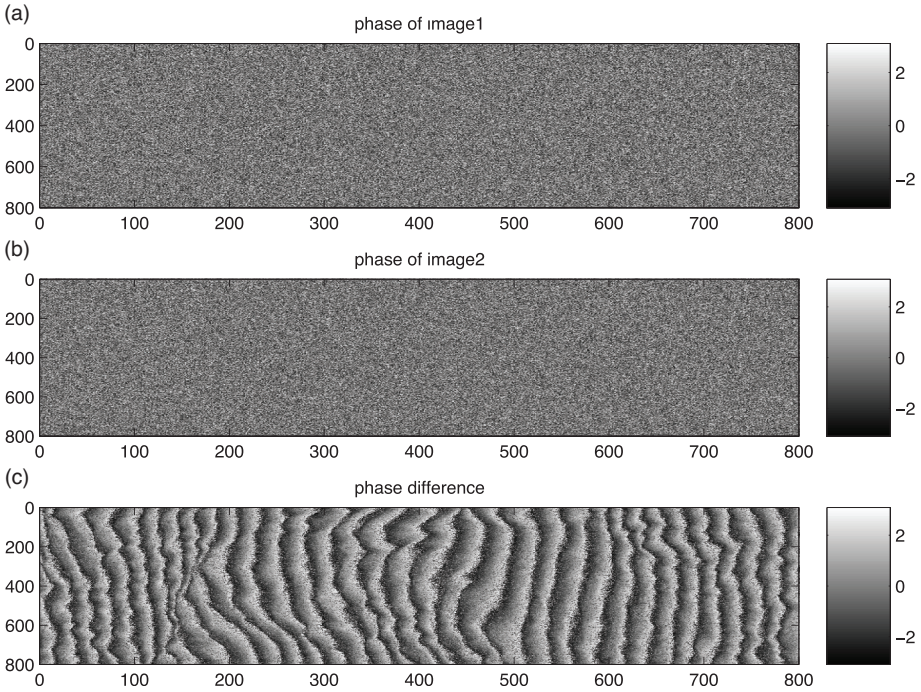

Figure 5.1 (a) The phase of a reference SLC file. (b) The phase of a repeat SLC file, and (c) the phase difference of repeat – reference SLC files calculated using Equations 5.2 and 5.3. The fringes across the interferogram are mostly due to the curvature of the Earth where the fringe rate is proportional to the perpendicular baseline between the reference and repeat images.

5.2 Contributions to Phase

The phase of an interferogram has many components as described in Equation 5.4.

$$\begin{aligned} \textit{phase} = {} & \textbf{Earth curvature} \text{ (almost a plane, known)} + \\ & \textbf{topographic phase} \text{ (broad spectrum)} + \\ & \textit{surface deformation} \text{ (broad spectrum, unknown)} + \\ & \textit{orbit error} \text{ (almost a plane, largely known)} + \\ & \textit{ionosphere advance} \text{ (often a plane or 20–40 km wavelength waves)} + \\ & \textit{troposphere delay} \text{ (power law, unknown)} + \\ & \textit{tides} \text{ (almost a plane, largely known)} + \\ & \textit{phase noise} \text{ (white spectrum, unknown)} \end{aligned} \tag{5.4}$$

A common task in InSAR analysis is to isolate the phase associated with surface deformation from all the other contributions. The largest known contribution comes

from the irregular shape of the Earth, which can be divided into an **Earth curvature component** and a **topography component**. In the remainder of this chapter, we show derivations of the phase and phase gradient due to Earth curvature, the *critical baseline, point scatterers*, and *phase due to topography*, as presented previously in Rosen et al. (1996); Joughin et al. (1996b); Sandwell and Price (1998). These derivations are useful for exposing concepts such as *parallel* and *perpendicular baseline*. However, this standard geometric model is not adequate for achieving high-accuracy results, especially for L-band large spatial baseline interferometry cases. We next derive the exact formulas that are implemented as *phasediff* in GMTSAR. These exact formulas are also conceptually and mathematically simpler than the approximate formulas, which are preferred in InSAR processing routines.

5.3 Phase due to Earth Curvature

The geometry of repeat-pass interferometry is shown in Figure 5.2.

The key parameters are:

ρ range from reference track to reflector
B total baseline distance between reference and repeat track
θ look angle
α angle between the baseline vector and the tangent plane

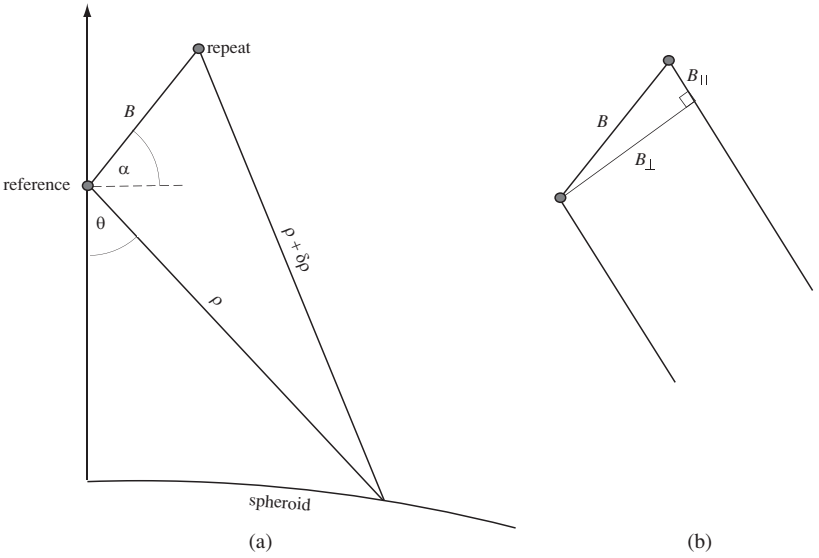

Figure 5.2 (a) Triangle for reference and repeat passes imaging the same point on the Earth. (b) The total baseline can be decomposed into parallel and perpendicular components.

The baseline B can be divided into parallel and perpendicular components given by

$$\begin{aligned} B_{\parallel} &= B \sin(\theta - \alpha) \\ B_{\perp} &= B \cos(\theta - \alpha) \end{aligned} \tag{5.5}$$

Because the look angle θ changes across the swath, the notion of a single perpendicular baseline for an interferometric combination is only an approximation. (*SAT_baseline* in GMTSAR computes the total baseline B as well as the angle α at 3 or more points along the image.) The phase difference ϕ to a point on the ground is related to the range difference $\delta\rho$.

$$\phi = \frac{4\pi}{\lambda}\delta\rho \tag{5.6}$$

where λ is the wavelength of the radar. The law of cosines provides the relationship among the repeat-pass range, the reference-pass range, the baseline length B, and the baseline orientation α as shown in Figure 5.2.

$$(\rho + \delta\rho)^2 = \rho^2 + B^2 - 2\rho B \sin(\theta - \alpha) \tag{5.7}$$

Under the assumption that $\delta\rho \ll \rho$, we have

$$\delta\rho = \frac{B^2}{2\rho} - B \sin(\theta - \alpha) \tag{5.8}$$

Furthermore, since $B \ll \rho$, the parallel ray approximation yields

$$\phi = \frac{-4\pi}{\lambda} B \sin(\theta - \alpha) \tag{5.9}$$

The phase difference depends on the parallel component of the baseline. The derivative of the phase with respect to range is

$$\frac{\partial\phi}{\partial\rho} = \frac{-4\pi}{\lambda} B \cos(\theta - \alpha) \frac{\partial\theta}{\partial\rho} \tag{5.10}$$

This phase gradient depends on two terms, the perpendicular component of the baseline $B_{\perp} = B\cos(\theta - \alpha)$ and the derivative of look angle with respect to range $\delta\theta/\delta\rho$. The perpendicular baseline varies slightly with look angle across a typical SAR image. The change in look angle usually increases with range, so $\delta\theta/\delta\rho > 0$. However, when the local terrain slope exceeds the look angle (actually the incidence angle), an increase in look angle does not produce a corresponding increase in range. This is the *layover* geometry where $\delta\theta/\delta\rho \leq 0$ (see Figure 7.2).

5.4 Look Angle and Incidence Angle for a Spherical Earth

In order to calculate the derivative of look angle with respect to range $\delta\theta/\delta\rho$, we first make the approximation that the Earth is locally spherical and then adjust the local radius of the Earth using the WGS84 ellipsoid 5.11. We note that there can

be large differences between the elliptical Earth model and the local radius for wide SAR swaths. This difference can produce topographic fringes in long-strip interferograms depending on the interferometric baseline. We address this issue later by including the ellipsoidal radius minus the local radius into a topographic correction term. The local Earth radius is given by

$$r_e(\varphi) = \left(\frac{\cos^2\varphi}{a^2} + \frac{\sin^2\varphi}{c^2} \right)^{-1/2} \tag{5.11}$$

where φ is latitude, and a and c are the equatorial (6 378 km) and polar (6 357 km) radii, respectively.

The radar look angle depends only on the local Earth radius r_e, the range to the sphere ρ, and the height of the spacecraft above the center of the Earth b as shown in Figure 5.3.

The law of cosines is used to calculate the look angle

$$\eta = \cos\theta = \frac{\left(b^2 + \rho^2 - r_e^2\right)}{2\rho b} \tag{5.12}$$

On a sphere, the incidence angle is greater than the look angle by the angle ψ.

To determine the derivative of the phase (5.10), we need to determine the derivative of the look angle with respect to range from Equation 5.12. An expression for the phase gradient due to Earth curvature is

$$\frac{\partial\phi}{\partial\rho} = \frac{-4\pi B}{\lambda\rho} \frac{\cos(\theta - \alpha)}{\sin\theta} \left(\cos\theta - \frac{\rho}{b} \right) \tag{5.13}$$

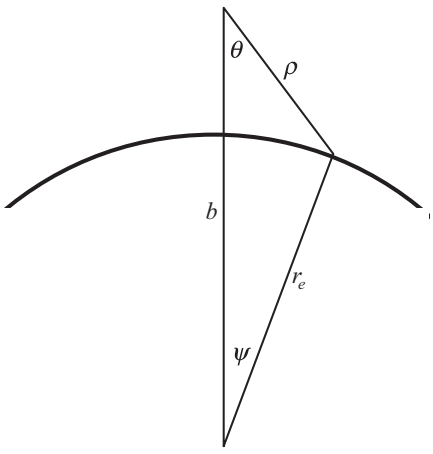

Figure 5.3 Triangle formed by the range ρ, radius of the Earth r_e, and spacecraft height b.

5.5 Critical Baseline

Consider a single range pixel of length $\Delta\rho = c\tau/2$. The phase of this pixel in the reference image is the vector sum of the phase from all scatterers in the pixel. The repeat image has the same scatterers but slightly different imaging geometry ($B > 0$). As a result, there are additional phase delays across the range cell, causing the sum of the phase from all scatterers to be different from the reference image. This is called baseline decorrelation. When the fringe rate across the interferogram exceeds 2π radians per range cell, the interferogram is completely decorrelated. This is the case of the *critical baseline*. To calculate the critical baseline, we start with Equation 5.13 and make a flat-Earth approximation $\rho/b = 0$. To avoid baseline decorrelation, change in phase with range must be less than

$$\frac{\partial\phi}{\partial\rho} = \frac{-4\pi B_\perp}{\lambda\rho}\frac{\cos\theta}{\sin\theta} < \frac{2\pi}{\Delta\rho} \tag{5.14}$$

The baseline where the fringe rate equals the critical value is

$$B_c = \frac{\lambda\rho}{c\tau}\tan\theta \tag{5.15}$$

For the parameters of the ERS satellite, the critical baseline is 1 100 m (Table 5.1). For topographic recovery, a baseline of about 1/4 critical is optimal. For change detection, a zero baseline is optimal but not usually available.

There is a second way to calculate the critical baseline. Consider a single ground range resolution pixel cell, which is related to the pulse length and the incidence angle $R_r = c\tau/(2\sin\theta)$. This cell is imaged from two positions separated by a perpendicular baseline (Figure 5.4). If the resolution cell contains only a single persistent scatterer at the center, the change in the viewing geometry does not change

Table 5.1 *Comparison of critical baseline (in km). ERS/Envisat – altitude = 790 km, wavelength = 56 mm. ALOS – altitude = 700 km, wavelength = 236 mm. Sentinel-1 – altitude = 700 km, wavelength = 55 mm, three look angles for each of the three subswaths. Shaded area is the most common mode for interferometry.*

Look angle	23°	34°	41°
ERS/Envisat 16 MHz	1.1	2.0	2.9
ALOS FBD 14 MHz	3.6	6.5	9.6
ALOS FBS 28 MHz	7.3	13.1	18.6
Sentinel-1 64 MHz	4.3	6.8	8.26

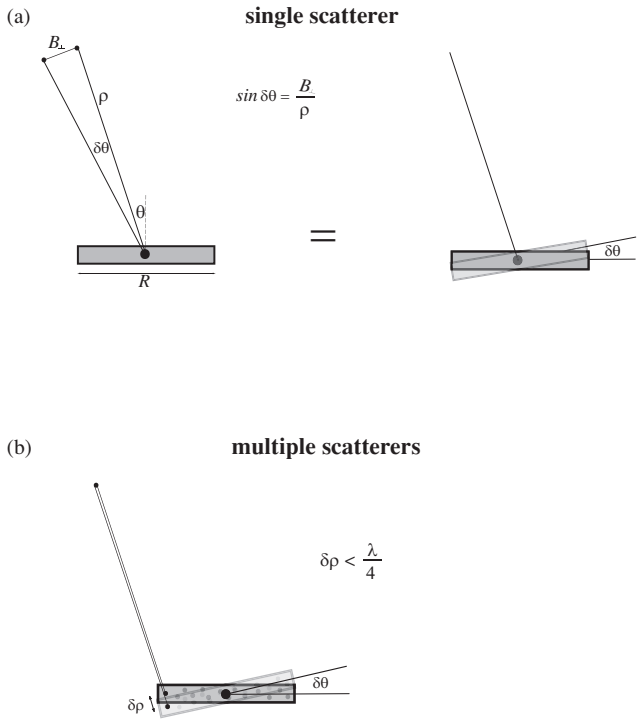

Figure 5.4 Diagrams showing the effects of changing viewing angle $\delta\theta$ for a resolution cell of length R. (a) point scatterer has no phase change with viewing angle. (b) has multiple scatterers where the vector sum of the phase will vary with viewing angle in a random way causing decorrelation.

the range to this single scatterer, and the pixel remains coherent. However, if there is a uniform distribution of persistent scatterers in the cell, the scatterers at the edges of the cell have a change in range of $\delta\rho = \frac{R_r}{2} \sin\delta\theta \cos\theta$. When $\delta\rho$ is less than a quarter of the wavelength, the phase shifts at the edge of the resolution cell do not destroy the correlation in the cell. Note that since the path delay is $2\delta\rho$, the phase delay is one half wavelength. It can be shown that the resulting critical baseline is the same as the formula found earlier

$$B_c = \frac{\lambda\rho}{2R_r \cos\theta} = \frac{\lambda\rho}{c\tau} \tan\theta \tag{5.16}$$

5.6 Approximate Phase due to Topography

We can use the approximate Equation 5.9 to calculate the topographic phase as well. The actual radius of the Earth (land), r, is usually greater than the radius of the spheroid r_e. The difference is the geometric elevation. The phase due to the actual topography can be expanded in a Taylor series about r_e

$$\phi(r) = \phi(r_e) + \left.\frac{\partial \phi}{\partial r}\right|_{r_e} (r - r_e) + \left.\frac{1\partial^2 \phi}{2\partial r^2}\right|_{r_e} (r - r_e)^2 + \cdots \tag{5.17}$$

Using Equations 5.9 and 5.12, we can calculate the first two derivatives. It turns out that the second derivative is about $(r - r_e)/r$ times the first derivative (i.e., 2.7/6 371 for our area), so we only need to keep the first two terms in the series. The first term is Equation 5.13, while the second term is

$$\frac{\partial \phi}{\partial r}(r_e) = \frac{-4\pi r_e}{\lambda \rho b} \frac{B \cos(\theta_e - \alpha)}{\sin \theta_e} \tag{5.18}$$

where θ_e is the look angle to the spheroid (5.12). The mapping of total unwrapped phase into elevation as a function of range is

$$(r - r_e) = \frac{-\lambda \rho b}{4\pi r_e} \frac{\sin \theta_e}{B \cos(\theta_e - \alpha)} (\phi - \phi_e) \tag{5.19}$$

Note that the unwrapped interferogram does not provide the complete phase difference $\phi - \phi_e$, given that there is an unknown constant of integration. While this formula is useful for demonstrating that the magnitude of the topographic phase correction is proportional to the perpendicular baseline, the formula is only an approximation. The more accurate approach used in the GMTSAR code is discussed in Section 5.8.

5.7 Topography from Single-Pass InSAR: SRTM

The Shuttle Radar Topography Mission (SRTM) used a single-pass interferometer with a fixed baseline to generate a near-global topography map of the Earth (60 N to 56 S) (Farr et al., 2007). The space shuttle was equipped with two receive antennas, one in the cargo bay and a second on a 60-m boom extending from the shuttle to form the fixed baseline. The transmit antenna was located in the shuttle bay and radar pulses were recorded by the two antennas after reflecting from the Earth's topography. The main advantage of a single-pass interferometer for topographic mapping is that the atmospheric and ionospheric phase delays cancel in the two SAR acquisitions, so the phase difference mainly reflects the topography. For a flat Earth geometry ($b/r_e = 1$), the sensitivity of the topography T to phase noise is

$$\frac{\partial T}{\partial \phi} = \frac{\lambda \rho \sin \theta_e}{2\pi B \cos(\theta_e - \alpha)}. \tag{5.20}$$

There is a factor of 2 difference from Equation 5.19 because there is only a phase difference from the reflected pulse, so this is a one-way phase difference measurement (Zebker et al., 1994). Inserting the values for the C-band radar at a nominal look angle of 45 degrees and a range to the surface of 330 km shows one fringe of phase corresponds to 108 m of topography. Since the radar was able to achieve

phase precision of 1/12 of a fringe, the nominal topography accuracy was 9 m. Note that the C-band radar does not reflect from the bare earth but from the canopy of vegetation as well as the tops of buildings. Nevertheless, this provides the optimal topography correction for C-band repeat-pass InSAR although will be suboptimal for L-band where the radar reflects deeper in the canopy or on the bare Earth.

5.8 Exact Phase due to Earth Curvature and Topography

In Sections 5.6 and 5.7, we provided approximate formulas for the phase changes from a curved Earth and local topography for a given perpendicular baseline. Here we derive the exact formulas. We start with the triangle shown in Figure 5.2. The law of cosines provides the relationship between the reference range ρ, the repeat range $\rho + \delta\rho$, the baseline length B, and the baseline orientation relative to the look angle $\theta - \alpha$. We can solve Equation 5.7 for $\delta\rho$

$$\delta\rho = \left[\rho^2 + B^2 - 2\rho B \sin(\theta - \alpha)\right]^{1/2} - \rho \tag{5.21}$$

and convert this to the phase correction $\phi = \frac{4\pi}{\lambda}\delta\rho$. The cosine of the look angle θ is given in Equation 5.12, which is valid for any Earth radius, such as the radius of a topographic reflector. In Chapter 3, we discussed an algorithm for mapping a topographic reflector from longitude, latitude, and height above the ellipsoid to range, azimuth, and topography $T(\rho, a)$ above a local spherical shape for the Earth. Using this information, we can combine the Earth curvature correction and the topographic phase correction into a single correction. The algorithm is:

1. Read a row of data from the reference and repeat SLC files, and assign every pixel in the reference image a range ρ and azimuth a.
2. Using the precise orbital information, compute the radius of the spacecraft orbit for the reference image $b(a)$, the length of the baseline $B(a)$, and the orientation of the baseline $\alpha(a)$.
3. Interpolate the topography to each range pixel and compute the look angle using the following formula from Equation 5.12.

$$\theta = \cos^{-1}\left\{\frac{\left(b^2 + \rho^2 - \left(r_e + T(\rho, a)\right)^2\right)}{2\rho b}\right\} \tag{5.22}$$

4. Using the look angle for each range pixel, calculate the phase correction to be applied to the repeat image using Equation 5.21 and the conversion from range to phase Equation 5.6.

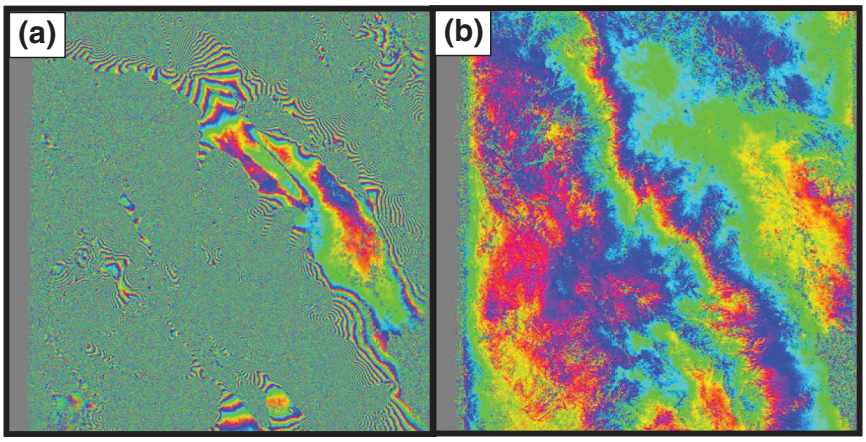

Figure 5.5 (a) A 1.95 km baseline interferogram with no topography correction has 120 fringes that need to be accurately removed. (b) Same interferogram corrected for topography phase using the exact Equations (5.21) and (5.22).

5. Multiply the repeat image by the complex phase and form the interferogram. Note this phase correction should be applied before any multilook averaging or filtering.

$$R(\mathbf{x}) + iI(\mathbf{x}) = C_2 C_1^* e^{i\phi} \tag{5.23}$$

6. Extract the interferometric phase, which is now corrected for both the Earth's curvature and the topographic phase.

$$(\phi_2 - \phi_1) = \tan^{-1}\left(\frac{I}{R}\right) \tag{5.24}$$

An example of a 1.95 km long baseline interferogram that was corrected for topographic phase is shown in Figure 5.5. There is 3 200 m of relief within this interferogram. As a result, there are 120 fringes in the full interferogram (Figure 5.5(a)) that need to be removed. The residual fringes (b) could be due to topography errors but could also be ionospheric or tropospheric delays.

5.9 Geocoding

Interferograms are naturally presented in the radar coordinates, where the x-axis corresponds to the range direction and the y-axis corresponds to the azimuth direction. It is challenging to relate the features in the radar coordinates with features seen in the latitude/longitude coordinates, because the ground features are often flipped, stretched, and rotated in the radar coordinates. Proper interpretation of interferograms requires the last step in the processing called *geocoding*, which transforms images in radar coordinates into geographic coordinates. In Section 3.7,

Table 5.2 *Lookup table for mapping from geographic to radar coordinates and vice versa.*

range	azimuth	elevation	longtitude	latitude
33484.3362	4554.8018	456.4585	-117.4900	35.7525
33462.4183	4553.8639	461.4579	-117.4891	35.7525
33438.8219	4552.9243	471.4572	-117.4883	35.7525
33415.9137	4551.9859	479.4566	-117.4875	35.7525
33395.6569	4551.0485	479.4560	-117.4866	35.7525
33376.7027	4550.1103	475.4554	-117.4858	35.7525
33356.4499	4549.1728	475.4548	-117.4850	35.7525
33335.8676	4548.2351	476.4543	-117.4841	35.7525
33315.2630	4547.2962	477.4537	-117.4833	35.7525
33294.6845	4546.3585	478.4531	-117.4825	35.7525

we discussed the use of the precise orbital information, along with a digital elevation model, to map between geographic and radar coordinates. We generated a lookup table called **trans**.**dat** to do the forward transformation. Now, we need to do the inverse transformation using the same table. A sample of the **trans**.**dat** file is provided in Table 5.2.

The first two columns of the file are the range and azimuth coordinates, column 3 is the height above the spheroid, and the last two columns are the longitude and latitude. The geocoding algorithm has the following steps:

1. Extract columns 1, 2, and 4 and use the GMT *surface* routine to make a grid of longitude versus range and azimuth. Repeat using columns 1, 2, and 5 to make a grid of latitude versus range and azimuth.
2. Extract wrapped phase observations from an interferogram.
3. Use the GMT command *grdtrack* along with the two grids of longitude versus range/azimuth, and latitude versus range/azimuth to create a table of longitude, latitude, and wrapped phase.
4. Establish the output pixel spacing in delta longitude and delta latitude to be 1/4 of the Gaussian filter wavelength to achieve full sampling. The longitude spacing is equal to the latitude spacing divided by the cosine of the latitude.
5. Use the GMT blockmedian routine to take the median value of the longitude, latitude, and wrapped phase in the previously established longitude and latitude bins.
6. Use the GMT command *xyz2grd* to populate the longitude, latitude, and wrapped phase grid. Note, some grid cells may not have entries. The empty locations will have the not-a-number flag. Also note that there is no interpolation of the regridded products. This is important for the wrapped phase, because there should be exact 2π discontinuities at the phase wrap boundaries and interpolation would blur the phase wrap.

5.10 Geocoded SLC InSAR Processing Strategy

In this chapter, we reviewed the key steps in the standard InSAR processing routines (Figure 5.6(a)): raw radar data from two satellite passes are processed into focused SAR images, and then delivered to end users. A user can use GMTSAR to coregister the radar images, and then cross-multiply the results to form an interferogram. The phase components due to Earth curvature and topography are estimated and removed based on the satellite orbit information and an existing DEM map. The geocoding step can be applied either on each individual flattened interferogram or the final surface deformation solutions derived from a stack of flattened interferograms. Zheng and Zebker (2017); Zebker (2017) proposed a geocoded SLC processing strategy (Figure 5.6(b)) that can be used to generate user-friendly radar image products for InSAR analysis:

1. Create a zero-Dopper SLC image for each scene using its orbit solutions.
2. Extract a DEM covering the region with desired postings (~SAR image resolution).

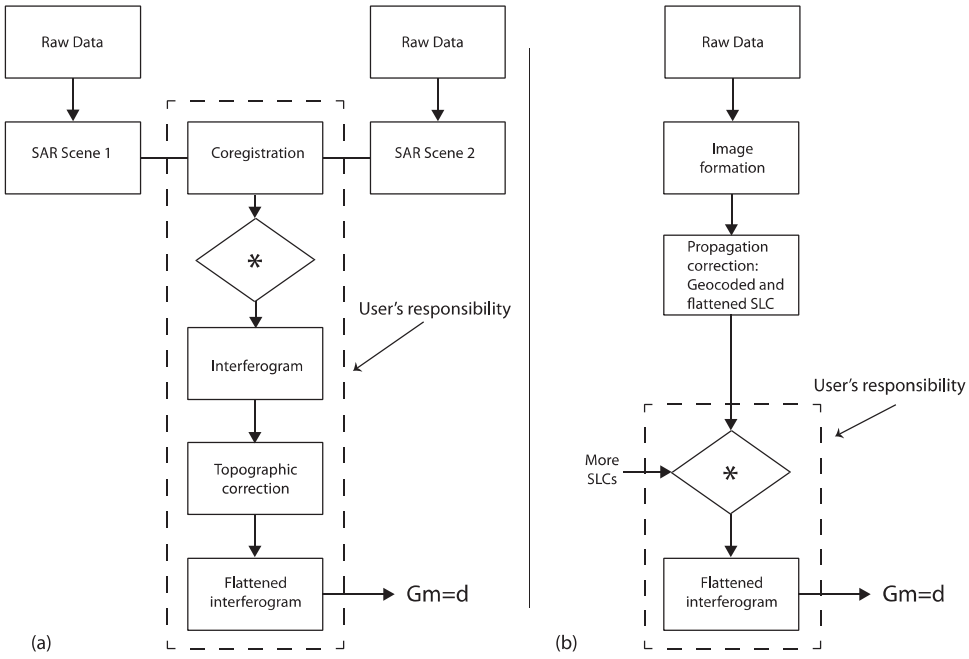

Figure 5.6 (a) Standard InSAR processing work flow that is commonly adopted by many InSAR processors. (b) Geocoded SLC InSAR processing work flow. Originally from Zebker (2017). Reprinted with permission from *IEEE Geoscience and Remote Sensing Letters*.

3. For each pixel in the DEM, find the corresponding zero-Doppler satellite observation location along the orbit.
4. Resample the SLC image to that DEM pixel, applying a phase correlation for the propagation distance from the sensor zero-Doppler point to the elevated surface point.

Compared to standard InSAR processing strategies, the topographic correction and geocoding steps are moved prior to the interferogram formation. Using this new processing architecture, interferograms can be generated with relatively low computational cost by simple cross-multiplication of pairs of these processed SLC radar images, which are automatically topography-corrected and geocoded. Depending on the desired spatial resolution, interferograms might be multi-looked to further reduce the overall storage needs and phase noise.

5.11 Problems

1. Develop a formula similar to Equation (5.12) for the incidence angle as a function of local Earth radius r_e, the range to the sphere ρ and the height of the spacecraft above the center of the Earth b.
2. Derive Equation (5.13). What happens when the change in phase with increasing range exceeds 2π radians per range resolution cell?
3. Give two reasons why the critical baseline for ALOS is more than 10 times longer than for ERS.
4. What happens to the phase of an interferogram in areas where the slope of the topography facing the radar exceeds the incidence angle of the radar?
5. Derive Equation (5.19). What is the correct zero level for the topography in this equation?